Natural convection in tilted cylindrical cavities embedded in rocks

F. Sánchez
Grupo de Medios Porosos y Granulados, Programa de Matemáticas y Computación, IMP Mexico D. F., 07730, Mexico

F. J. Higuera and A. Medina
E.T.S. Ingenieros Aeronáuticos, UPM, Madrid 28040, Spain
(Received 30 June 2004; revised manuscript received 28 February 2005; published 27 June 2005)

This paper presents a theoretical investigation of the low Rayleigh number conjugate natural convection in a slender tilted cylindrical cavity which is embedded in a solid that is subject to a uniform vertical temperature gradient. Two cases have been analyzed; a fluid-filled cavity and a cavity filled with a fluid-saturated porous medium. The temperature of the solid and the velocity, temperature, and pressure in the cavity have been determined by analytically solving the coupled problems within and around the cavity. The effect of the ratio of the thermal conductivity of the material in the cavity to the thermal conductivity of the solid on the structure of the convection flow is discussed. The theoretical results for convection in the fluid-filled cavity are shown to be in good agreement with experimental PIV measurements.

DOI: 10.1103/PhysRevE.71.066308 PACS number(s): 44.25.+f, 44.30.+v, 47.55.Mh

I. INTRODUCTION

A vertical temperature gradient in a solid always induces a natural convection flow in fluid-filled tilted slots embedded in the solid, irrespective of the strength of the temperature gradient and the viscosity of the fluid. This is because the isotherms would not be horizontal in the fluid at rest, except in the particular case when the thermal conductivity of the fluid coincides with the thermal conductivity of the solid. A number of theoretical and experimental studies [1–8] have addressed this natural convection flow in very slim slots. These systems have been assumed to be simple and ideal representations of fractures occurring in rocks and other brittle materials. The knowledge thus gained is of enormous importance to understand the diagenetic processes [3,4], the migration of water and oil in subterranean reservoirs [3,9] and the ice formation from seawater [10,11], among other relevant phenomena.

In this paper, we analyze the conjugate natural convection within tilted, cylindrical cavities embedded in impervious rocks subject to a vertical temperature gradient. Cavities filled with a fluid and with a fluid-saturated porous medium are considered. In addition to its inherent physical interest, this problem appears frequently in controlled studies of ice formation [10,11] and in the oil industry, both when pipes are embedded into subterranean reservoirs to extract fluids and in connection with hot-fluid-injection oil-recovery methods [9]. In the last two cases the thermal conductivity of the solid is large compared with that of the fluid or the effective thermal conductivity of the saturated porous material which fills the cavity, but due to the large variety of possible applications, the thermal conductivity ratio may span a wide range of values, both large and small compared with unity. The present work presents analytical solutions for the velocity, pressure and temperature for small Rayleigh numbers. We deal with the general case where the rock thermal conductivity is different from the thermal conductivity of the material in the cavity, and analyze the coupled thermal problems within and around the tilted cavity. The results for the fluid-filled cavity have been tested in an experiment carried out in a tilted, silicon oil-filled cavity embedded in a plexiglas block which is kept in contact with two blocks of copper at different temperatures, above and below the plexiglas block. The agreement between the experimental data and the theoretical profiles for such a case allows to conclude that our model describes well the small Rayleigh number thermal convection in long cylindrical cavities.

The paper is organized as follows. The thermal problem in the rock is formulated in Sec. II. In Sec. III the thermal and fluid flow problem within a very slender cylindrical cavity is analyzed and solved together with the thermal problem in the surrounding rock, first for a fluid-filled cavity and then for a cavity containing a fluid-saturated porous medium. Closed-form analytical solutions for the temperature, velocity and pressure are obtained in both cases. Experiments carried out for a fluid-filled cavity, where the flow visualization is possible, are discussed in Sec. IV. These experimental results validate our theoretical approach. Finally, the main conclusions of the work are presented in Sec. V.

II. TEMPERATURE DISTRIBUTION IN THE ROCK

Consider a cylindrical cavity of length $2L$ and radius a in an infinite impermeable rock. The axis of the cavity is inclined at an angle γ to the horizontal. The thermal conductivity of the material filling the cavity is k_f and the thermal conductivity of the rock is k_s. The parameters $\varepsilon = a/L$ (aspect ratio of the cavity) and $\delta = k_f/k_s$ will be used in that follows. In actual geophysical systems, these two parameters may span wide ranges of values, both large and small compared with unity. The cylindrical coordinates (r^*, ϕ, x^*) of Fig. 1(b) will be used. Here x^* is the distance along the axis of the cavity increasing upward from the central section of the cav-

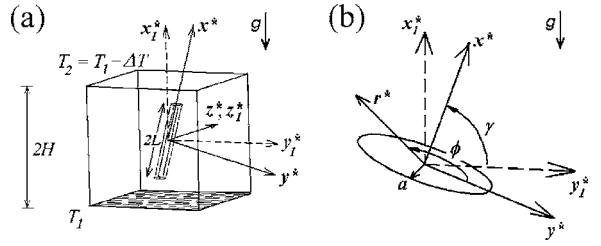

FIG. 1. Schematic of the physical model and coordinate systems.

ity, which therefore extends from $x^*=-L$ to $x^*=L$, and the angle ϕ is measured from a vertical plane.

Assume that a uniform vertical temperature gradient G^* is established in the rock. In the absence of the cavity, the temperature T_S of the rock would vary linearly with the vertical distance x_1^* of Fig. 1 as $T_S=T_\infty(x_1^*)=G^*x_1^*+T_0$, where T_0 is the temperature at $x_1^*=0$. The temperature gradient G^* can be positive or negative.

The following dimensionless variables will be used

$$r=\frac{r^*}{a},\quad x=\frac{x^*}{L},$$

$$\theta_s=\frac{T_S-T_0}{T_0},\quad G=\frac{aG^*}{T_0}. \tag{1}$$

In terms of these variables, the dimensionless temperature of the rock far from the cavity is

$$\theta_\infty=G\left(\frac{x}{\varepsilon}\sin\gamma-r\cos\gamma\cos\phi\right). \tag{2}$$

The presence of the cavity changes the temperature of the rock, which must satisfy

$$\nabla^2\theta_s=0 \tag{3}$$

with the boundary condition $\theta_s\to\theta_\infty$ far from the cavity and conditions at the surface of the cavity which express the continuity of the temperature and the heat flux. These conditions couple the thermal problem in the rock with the thermal problem of the material inside the cavity.

III. CONVECTIVE FLOW

Once the problem of the temperature distribution in the rock has been defined, we may focus on the natural convection flow arising in the cavity. As noticed previously for slim tilted fractures embedded in solids [1,7,8], such a flow must necessarily exist when the solid is under a vertical temperature gradient and the thermal conductivity ratio is not equal to 1, no matter how small the temperature gradient is. This is the case because the isotherms in the fluid at rest are not horizontal when $\delta\neq 1$ and the cavity is neither horizontal nor vertical.

The different problem of the onset of convection in a vertical cylindrical cavity has been extensively studied for both fluid-filled cavities [12,13] and fluid-saturated porous cavities [14,15]. There are well-known critical Rayleigh numbers for each of these cases, at variance with the case of tilted cavities addressed in this paper. Likewise, the horizontal cylindrical cavities have been widely analyzed for many heating configurations. Those studies include the fluid-filled cavity [16] and the saturated porous cavity [17].

It is worth to note that the present study is restricted to the case when the aspect ratio and the Rayleigh number are both small. Under these conditions, there would not exist any convective flow if the slim cylindrical cavity were either vertical or horizontal [12,15,16].

The following analysis considers that the fluid has kinematic viscosity ν, density ρ, thermal expansion coefficient β, and thermal diffusivity α. A steady-state flow is assumed and the Boussinesq approximation is applied. The cases of a fluid-filled cavity and a cavity filled with a fluid-saturated porous medium are discussed separately.

A. Fluid-filled cavity

1. General formulation

The convective motion within the cavity is governed by the continuity, momentum and energy equations, which in a nondimensional form are

$$\boldsymbol{\nabla}\cdot\mathbf{u}=0, \tag{4}$$

$$\mathrm{Ra}(\mathbf{u}\cdot\boldsymbol{\nabla})\mathbf{u}=-\boldsymbol{\nabla}P+\mathrm{Pr}\nabla^2\mathbf{u}+\frac{\mathrm{Pr}}{G}(\theta_i-\theta_\infty)\mathbf{i}_g, \tag{5}$$

$$\mathrm{Ra}(\mathbf{u}\cdot\boldsymbol{\nabla})\theta_i=\nabla^2\theta_i, \tag{6}$$

with the boundary conditions of nonslip and continuity of the temperature and the heat flux at the surface of the cavity:

$$\mathbf{u}=\mathbf{0},\quad \theta_i=\theta_s \text{ and } \delta\frac{\partial\theta_i}{\partial n}=\frac{\partial\theta_s}{\partial n}\quad \text{at } r=1,\ |x|<1 \text{ and}$$

$$x=\pm 1, r<1. \tag{7}$$

Here $\mathbf{i}_g$ is a unit upward pointing vector, $\mathbf{u}=(u_r,u_\phi,u_x)$ is the velocity of the fluid, P is a modified pressure which takes care of the hydrostatic term, and Pr and Ra are the Prandtl and Rayleigh numbers. The nondimensional variables are defined as follows:

$$u_r=\frac{u_r^*a}{\alpha\mathrm{Ra}},\quad u_\phi=\frac{u_\phi^*a}{\alpha\mathrm{Ra}},\quad u_x=\frac{u_x^*a}{\alpha\mathrm{Ra}},\quad P=\frac{P^*a^2}{\rho\alpha^2\mathrm{Ra}},$$

$$\theta_i=\frac{T_i-T_0}{T_0},\quad \mathrm{Pr}=\frac{\nu}{\alpha},\quad \mathrm{Ra}=\frac{g\beta a^4|G^*|}{\alpha\nu} \tag{8}$$

and, in terms of the dimensionless x and r introduced in (1),

$$\boldsymbol{\nabla}=\mathbf{i}_r\frac{\partial}{\partial r}+\mathbf{i}_\phi\frac{1}{r}\frac{\partial}{\partial\phi}+\mathbf{i}_x\varepsilon\frac{\partial}{\partial x}, \tag{9}$$

$$\nabla^2=\frac{1}{r}\frac{\partial}{\partial r}\left(r\frac{\partial}{\partial r}\right)+\frac{1}{r^2}\frac{\partial^2}{\partial\phi^2}+\varepsilon^2\frac{\partial^2}{\partial x^2}. \tag{10}$$

Finally $\partial/\partial n$ in (7) denotes the derivative normal to the surface of the cavity.

2. Zero Rayleigh number

We begin discussing the case Ra=0 in which the energy equation in the cavity, Eq. (6), reduces to

$$\nabla^2 \theta_i = 0. \tag{11}$$

The temperatures of the rock and the cavity are then of the form $\theta_s = \theta_\infty - G\cos\gamma\cos\phi f_1(r,x) + G\sin\gamma f_2(r,x)$ and $\theta_i = \theta_\infty - G\cos\gamma\cos\phi f_3(r,x) + G\sin\gamma f_4(r,x)$. Carrying these expressions to (3) and (11) we find

$$\nabla_0^2 f_1 - \frac{1}{r^2} f_1 = 0 \text{ in the rock},$$

$$\nabla_0^2 f_3 - \frac{1}{r^2} f_3 = 0 \text{ in the cavity},$$

$$f_1 = 0 \text{ for } (x,r) \to \infty,$$

$$f_1 = f_3, \quad \frac{\partial f_1}{\partial r} - \delta \frac{\partial f_3}{\partial r} = \delta - 1 \text{ at } r = 1,\ |x| < 1,$$

$$f_1 = f_3, \quad \frac{\partial f_1}{\partial x} = \delta \frac{\partial f_3}{\partial x} \text{ at } x = \pm 1,\ r < 1 \tag{12}$$

and

$$\nabla_0^2 f_2 = 0 \text{ in the rock},$$

$$\nabla_0^2 f_4 = 0 \text{ in the cavity},$$

$$f_2 = 0 \text{ for } (x,r) \to \infty,$$

$$f_2 = f_4, \quad \frac{\partial f_2}{\partial r} = \delta \frac{\partial f_4}{\partial r} \text{ at } r = 1,\ |x| < 1,$$

$$f_2 = f_4, \quad \frac{\partial f_2}{\partial x} - \delta \frac{\partial f_4}{\partial x} = \frac{\delta - 1}{\varepsilon} \text{ at } x = \pm 1,\ r < 1 \tag{13}$$

with the additional conditions that the functions f_1 to f_4 should be regular at $r=0$. Here

$$\nabla_0^2 = \frac{1}{r}\frac{\partial}{\partial r}\left(r \frac{\partial}{\partial r}\right) + \varepsilon^2 \frac{\partial^2}{\partial x^2}. \tag{14}$$

Solving (12) and (13) we would find exact solutions of the coupled conduction problem in the rock and within the cavity for the limit case Ra=0.

Problems (12) and (13) can be further simplified noticing that for many cases of practical interest, particularly in the geophysical context, the cavities are slender ($\varepsilon \ll 1$). Two different regions can then be distinguished. End effects due to the finite length of the cavity are confined to a region of characteristic size a [or $r=O(1)$ in dimensionless variables] around each end of the cavity, while the temperature in the rest of the cavity and the surrounding rock is as if the cavity were infinitely long. We are interested here only in the latter region, which is where the main flow takes place. The small regions around the ends of the cavity need not be analyzed. The solutions of (12) and (13) for an infinitely long cavity are $f_1 = (1-\delta)/(1+\delta)r$, $f_3 = (1-\delta)r/(1+\delta)$, and $f_2 = f_4 = 0$. Thus, in the case Ra=0, the dimensionless temperature in the solid around the cylindrical cavity but away from its ends is

$$\theta_{s_0} = G\left[\frac{x}{\varepsilon}\sin\gamma - \cos\gamma\cos\phi\left(r + \frac{1-\delta}{1+\delta}\frac{1}{r}\right)\right], \tag{15}$$

and the dimensionless temperature within the cavity but away from its ends is

$$\theta_{i_0} = G\left[\frac{x}{\varepsilon}\sin\gamma - \cos\gamma\cos\phi\frac{2r}{1+\delta}\right]. \tag{16}$$

The velocity and reduced pressure of the natural convection flow induced in the cavity by the temperature distribution (16) can now be determined. Since u_ϕ and u_r are of the order of εu_x and $\varepsilon \ll 1$, the main flow is one-dimensional along the axis of the cavity, $u_x = u_x(r,\phi)$, and Eq. (5) reduces to

$$0 = -\frac{\partial P}{\partial x} + \mathrm{Pr}\nabla^2 u_x + \frac{\mathrm{Pr}\sin\gamma}{|G|}(\theta_i - \theta_\infty), \tag{17}$$

with the boundary conditions $u_x = 0$ at $r=1$, $u_x < \infty$ at $r=0$, and the condition of zero through flow, $\int_0^1 \int_0^{2\pi} u_x r d\phi dr = 0$. The solution of this problem has the form $P=0$, $u_x = f(r)\cos\phi$. From Eq. (17), it follows that

$$\frac{d^2 f}{dr^2} + \frac{1}{r}\frac{df}{dr} - \frac{f}{r^2} = \pm\sin\gamma\cos\gamma\frac{1-\delta}{1+\delta}r, \tag{18}$$

whose solution with $f(0) < \infty$ and $f(1) = 0$ is $f = \pm\frac{1}{8}\sin\gamma\cos\gamma((1-\delta)/(1+\delta))r(r^2-1)$. Thus

$$u_{x_0} = \pm\frac{\sin\gamma\cos\gamma\cos\phi}{8}\frac{1-\delta}{1+\delta}r(r^2-1). \tag{19}$$

The plus sign on Eq. (19) is used for positive thermal gradients, $G>0$, and the minus sign is used for negative thermal gradients, $G<0$.

3. Small Rayleigh numbers

The previous solutions for the temperature and the velocity can be corrected in order to consider the effect of a small but nonzero Rayleigh number. When ε is small and $\mathrm{Ra} \neq 0$ Eq. (6) simplifies to

$$\varepsilon \mathrm{Ra}\, u_x \frac{\partial \theta_i}{\partial x} = \nabla^2 \theta_i \tag{20}$$

away from the ends of the cavity.

Rather than formally introducing a perturbation expansion in powers of Ra, we may use an equivalent *iteration* method to find the effects of the convective flow on the temperature distribution. A first-order correction to the solution for Ra=0 can be computed by using Eqs. (16) and (19) to evaluate the left-hand side of Eq. (20). This equation becomes then

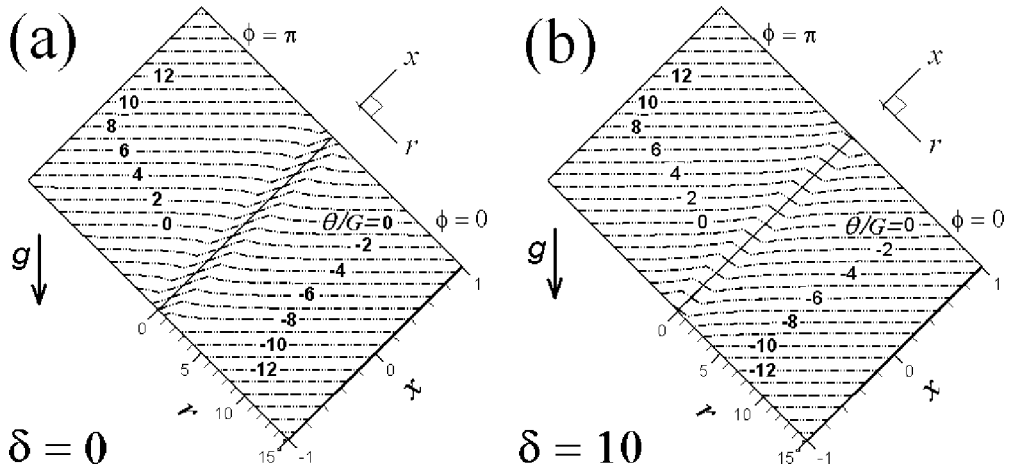

FIG. 2. Effect of δ on the dimensionless temperature distribution scaled with G inside and around a tilted cavity. These slices correspond to planes $\phi=0$ and $\phi=\pi$, when $\gamma=\pi/4$.

$$\pm\frac{1}{8}G\mathrm{Ra}\sin^2\gamma\cos\gamma\frac{1-\delta}{1+\delta}r(r^2-1)\cos\phi=\nabla^2\theta_i, \quad (21)$$

to be solved with boundary conditions that express the continuity of the temperature and the heat flux at the surface of the cavity. Writing again the temperature of the rock in the form $\theta_s=\theta_\infty-G\cos\gamma\cos\phi f_1(r)$ and the temperature within the cavity in the form $\theta_i=\theta_\infty-G\cos\gamma\cos\phi f_3(r)$ (for an infinitely long cavity), we can easily find differential equations and boundary conditions for the functions f_1 and f_3. The corrected dimensionless temperature distributions in the solid and within the cavity obtained by solving such equations are

$$\theta_s=\theta_{s_0}+\lambda\frac{\delta G\cos\gamma\cos\phi}{96(1+\delta)}\frac{1}{r}, \quad (22)$$

$$\theta_i=\theta_{i_0}+\lambda G\cos\gamma\cos\phi\left[\frac{(1+2\delta)r}{96(1+\delta)}+\frac{r^3(r^2-3)}{192}\right], \quad (23)$$

where θ_{s_0} and θ_{i_0} are the leading order temperatures given by (15) and (16), and λ is a convection parameter defined as

$$\lambda=\mathrm{Ra}G\frac{1-\delta}{1+\delta}\sin^2\gamma. \quad (24)$$

On the other hand, the corrected velocity induced in the cavity by the temperature distribution (23) is determined by Eq. (17) with the nonslip and zero through flow conditions used before. Again, the solution of this problem can be sought in the form $P=0$, $u_x=f(r)\cos\phi$. After some algebra we find

$$u_x=u_{x_0}\pm\frac{\lambda\sin\gamma\cos\gamma\cos\phi r}{768}\left[\frac{r^4}{2}-\frac{r^6}{12}-\frac{1+2\delta}{1+\delta}r^2+\frac{7+19\delta}{12(1+\delta)}\right], \quad (25)$$

where u_{x_0} is the leading order velocity given by (19). Again, the plus sign on Eq. (25) is used for positive thermal gradients, $G>0$, and the minus sign is used for negative thermal gradients, $G<0$.

Figure 2 shows local slices of the dimensionless temperature distribution scaled with G inside and around a tilted, infinitely long cavity. This figure shows the effect of the thermal conductivity ratio, δ, when $\gamma=\pi/4$. Both slices in Fig. 2 show the plane $\phi=0,\pi$, and correspond to the basic solutions of $\lambda=0$, which are only slightly modified for small values of λ. Isotherms labeled as θ/G correspond to θ_{s_0}/G when $r\geqslant 1$ [Eq. (15)] and to θ_{i_0}/G for $r<1$ [Eq. (16)]. If the solid thermal conductivity is either very large or very small compared with that corresponding to the material within the cavity, there is an abrupt change experimented by the isotherms and the surface of the cavity is easily identified. The effect of the cavity on the isotherms in the rock extends to distances from the cavity wall of the order of its radius. The effect of the cavity on the isotherms diminishes when the thermal conductivities become of the same order, and disappear when $\delta=1$. Then the isotherms are horizontal and no convection arises in the cavity. If the thermal conductivity of the solid is lower than the thermal conductivity of the fluid in the cavity ($\delta>1$), the change of the isotherms near and within the cavity is opposite to that of the case $\delta<1$ [see Fig. 2(b)], and such a change becomes more pronounced when δ increases.

The velocity distribution in a cross section of the cavity is shown in Fig. 3 for $\lambda=0$. Plotted in this figure are contours of the dimensionless longitudinal velocity u_{x_0} divided by $\pm\frac{1}{8}\sin\gamma\cos\gamma(1-\delta)/(1+\delta)$. There is a counter flow within the cavity and the contour of zero velocity is at the middle of the circular section. The velocity profiles on the plane $\phi=0,\pi$ are shown in Fig. 4 for different values of the parameter λ, which measures the effect of the convective transport.

The effect of the thermal conductivity ratio δ on the magnitude of the velocity is notable. If the thermal conductivity ratio diminishes, the longitudinal velocity increases and reaches its maximum when $\delta\to 0$. As δ augments the longitudinal velocity decreases and when $\delta=1$ there is no convection flow. If $\delta>1$, the longitudinal velocity changes its ori-

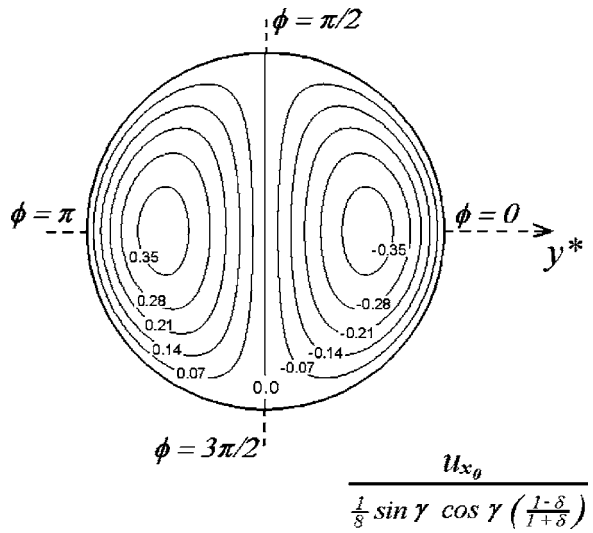

FIG. 3. Isovelocity contours on the transversal cross section. The contours correspond to the dimensionless longitudinal velocity u_{x_0} scaled with $\frac{1}{8}\sin(\gamma)\cos(\gamma)(1-\delta)/(1+\delta)$.

entation and its module augments when δ increases.

The dimensionless heat flux, $(\partial\theta_i/\partial r)_{r=1}$ normal to the cavity surface can be easily found from Eq. (23). The local dimensionless heat flux divided by $G\cos\gamma$ is shown in Fig. 5, where the effect of the thermal conductivity ratio is shown for the limit case of $\lambda=0$. The heat flux normal to the cavity surface is maximum when $\delta\to 0$ and diminishes as δ increases, so that if $\delta\to\infty$ then $(\partial\theta_i/\partial r)_{r=1}\to 0$. Figure 2(a) shows that when $\delta\to 0$ the isotherms experiment an abrupt change on the surface of the cavity; when $\delta=1$ the isotherms are horizontal but since the r axis is not horizontal then $(\partial\theta_i/\partial r)_{r=1}\neq 0$; and when $\delta\to\infty$ (the solid is a poor conductor) the isotherms within the cavity become normal to the cylindrical surface, leading to $(\partial\theta_i/\partial r)_{r=1}=0$. See Fig. 2(b).

Figure 6 shows the dimensionless heat flux normal to the cavity for different values of λ when $\delta=0.1$. This figure describes the effect of the convective transport on the heat transfer through the cavity. As it could be expected, the heat transfer for small Rayleigh numbers is slightly larger than

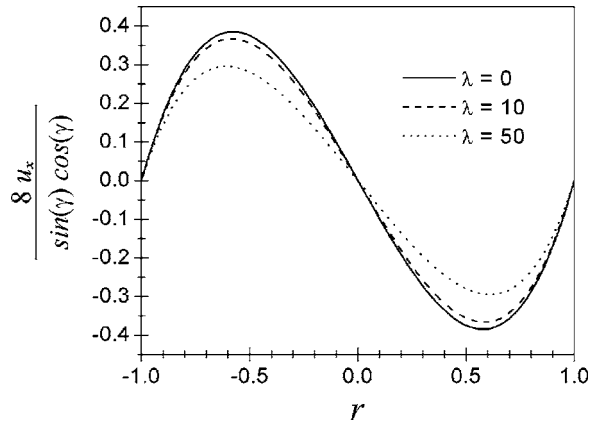

FIG. 4. Effect of the convection parameter λ on the flow velocity. Velocity profiles shown here correspond to the vertical plane $\phi=0$ and for cases $G>0$ when $\delta=0$.

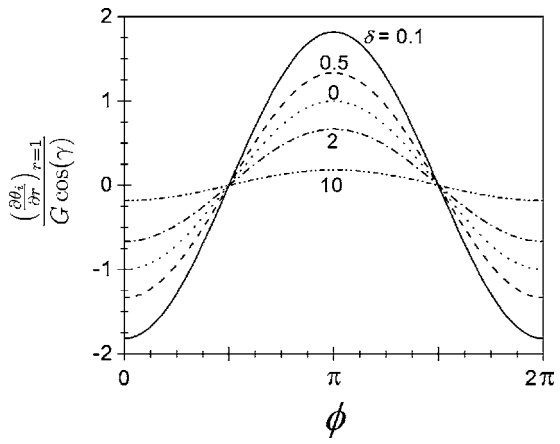

FIG. 5. Effect of the thermal conductivity ratio δ on the local dimensionless heat flux normal to the cavity surface when $\lambda=0$.

that corresponding to the pure conduction condition where $\lambda=0$.

B. Porous medium filled cavity

1. General formulation

The natural convection flow in the fluid-saturated porous cavity is governed by the continuity equation, the Darcy's law, and the energy equation. In the Boussinesq approximation and nondimensional form, the flow in the cavity obeys

$$\nabla\cdot\mathbf{u}=0, \tag{26}$$

$$\mathbf{u}=-\nabla P+\frac{1}{G}(\theta_i-\theta_\infty)\mathbf{i}_g, \tag{27}$$

$$\mathrm{Ra}(\mathbf{u}\cdot\nabla)\theta_i=\nabla^2\theta_i, \tag{28}$$

where $\mathbf{i}_g$ is the unit vector that points the direction of the gravitational acceleration, $\mathbf{u}=(u_r,u_\phi,u_x)$ is the filtration velocity field, P is a modified pressure which takes care of the hydrostatic term, Ra is the Rayleigh number, the operators ∇ and ∇^2 are defined in Eqs. (9) and (10), and the dimensionless variables are defined as follows:

$$u_r=\frac{u_r^* a}{\alpha\mathrm{Ra}},\quad u_\phi=\frac{u_\phi^* a}{\alpha\mathrm{Ra}},\quad u_x=\frac{u_x^* a}{\alpha\mathrm{Ra}},$$

$$P=\frac{P^* aK}{\rho\nu\alpha\mathrm{Ra}},\quad \mathrm{Ra}=\frac{g\beta a^2K|G^*|}{\alpha\nu}, \tag{29}$$

where K is the permeability of the porous medium (in units of $[\mathrm{m}^2]$), and α is its effective thermal diffusivity.

2. Zero Rayleigh number

As before, we get a first approximation considering the case when $\mathrm{Ra}\to 0$, then the energy equation in the porous cavity, Eq. (28), simplifies to the same one stated by Eq. (11), which is coupled with the thermal problem in the rock, Eq. (3), by the boundary conditions at the surface of the

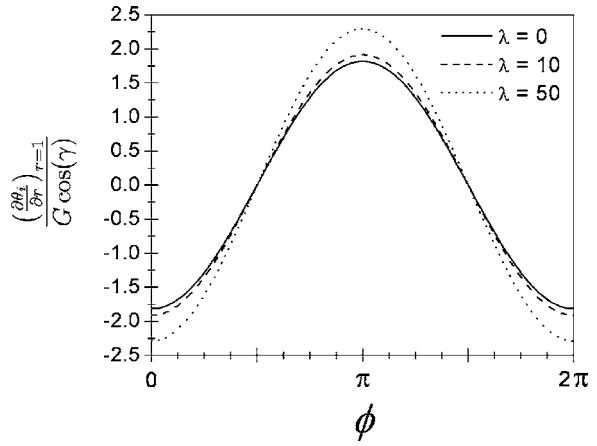

FIG. 6. Effect of the convection parameter λ on the local dimensionless heat flux normal to the cavity surface when $\delta=0.1$.

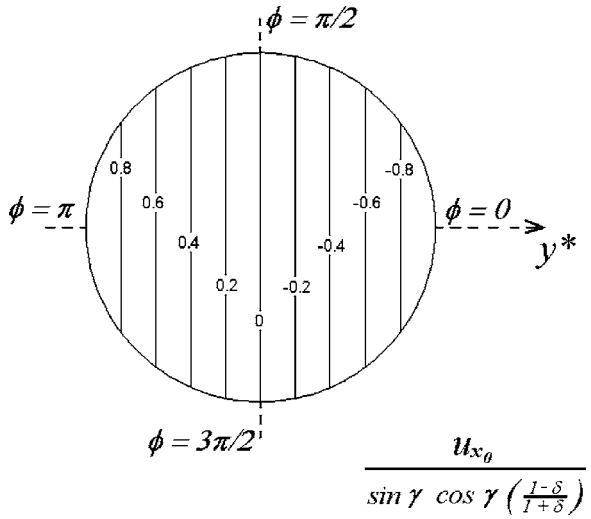

FIG. 7. Isovelocity contours within the porous cavity on the transversal cross section. Shown contours correspond to the dimensionless filtration velocity u_{x_0} scaled with $\sin(\gamma)\cos(\gamma)(1-\delta)/(1+\delta)$.

cavity which express the continuity of the temperature and the heat flux. This is exactly the same problem considered as the first approximation in the case of a fluid-filled cavity. Consequently, under the assumption that $\varepsilon \ll 1$, the basic solutions for the temperature distributions around and within the porous cavity are the same already found as the first approximation in the previous section, Eqs. (15) and (16). Additionally, a basic solution of the filtration velocity and reduced pressure within the porous cavity can be determined. Again u_ϕ and u_r are of the order of εu_x and $\varepsilon \ll 1$, so, the main flow is one-dimensional along the axis of the cavity, $u_x(r,\phi)$, and Eq. (27) reduces to

$$u_x = -\varepsilon \frac{\partial P}{\partial x} + \frac{\sin\gamma}{|G|}(\theta_i - \theta_\infty). \tag{30}$$

Carrying the temperature solution of Eq. (16) to Eq. (30) and using the zero net flux condition, we found that the solution of this problem is of the form $P=0$, $u_x=f(r)\cos(\phi)$. Then, it follows that the basic solution of the filtration velocity is

$$u_{x_0} = \mp \sin\gamma\cos\gamma\cos\phi\frac{1-\delta}{1+\delta}r. \tag{31}$$

The minus sign in Eq. (31) is used for positive thermal gradients, $G>0$, and the plus sign is used for negative thermal gradients, $G<0$.

3. Small Rayleigh numbers

The basic solutions can be corrected in order to consider the effect of a small both nonzero Rayleigh number when $\varepsilon \ll 1$. When ε is small and $\mathrm{Ra} \neq 0$ Eq. (28) simplifies to the same problem stated by Eq. (20). Iteration was used again as the way of finding a successive approximation that considers the first-order effects of the convective flow on the temperature distribution. The basic solutions, Eqs. (16) and (31), were used to evaluate the left-hand side of Eq. (20), and solve again. Thus, such a equation becomes

$$\mp \mathrm{Ra}G\sin^2\gamma\cos\gamma\cos\phi\frac{1-\delta}{1+\delta}r = \nabla^2\theta_i, \tag{32}$$

with the boundary conditions that express the continuity of the temperature and the heat flux at the surface of the cavity. Using again the aforementioned methodology, the corrected dimensionless temperature distributions in the solid slab and within the cylindrical porous cavity respectively are

$$\theta_s = \theta_{s_0} + \lambda\frac{G\cos\gamma\cos\phi}{4r}\left(\frac{\delta}{1+\delta}\right), \tag{33}$$

$$\theta_i = \theta_{i_0} + \lambda\frac{G\cos\gamma\cos\phi}{8}\left[\frac{1+3\delta}{1+\delta}r - r^3\right], \tag{34}$$

where λ obeys the same definition as in Eq. (24).

The corrected filtration velocity induced in the cavity by the temperature distribution (34) is determined by Eq. (30) with the aforementioned boundary conditions. Again, the solution of this problem is of the form $P=0$, $u_x=f(r)\cos\phi$. So, it follows that

$$u_x = u_{x_0} \mp \lambda\frac{\sin\gamma\cos\gamma\cos\phi}{8}\left[r^3 - \frac{1+3\delta}{1+\delta}r\right], \tag{35}$$

where the minus sign is used for positive thermal gradients, $G>0$, and the plus sign is used for negative thermal gradients, $G<0$.

For small values of λ, the dimensionless temperature distribution inside and around the tilted porous cavity looks quite similar to plots in Fig. 2.

A typical plot of the dimensionless filtration velocity distribution within the porous cavity is presented in Fig. 7. There, the isovelocity contours on the transversal cross-section corresponding to the limit case of $\lambda=0$ are shown. Numerical values of the contours in Fig. 7 correspond to the dimensionless longitudinal filtration velocity within the cav-

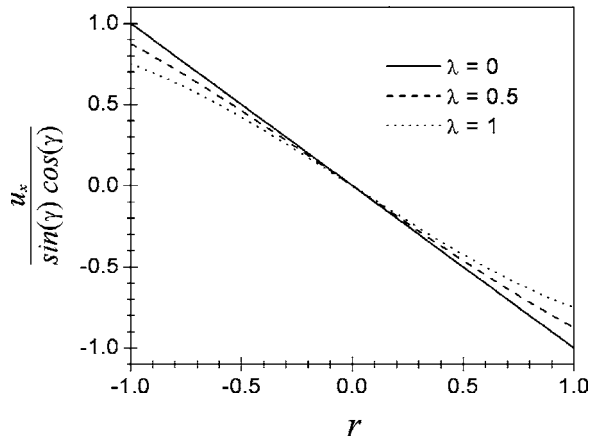

FIG. 8. Effect of the convection parameter λ on the filtration velocity in the porous cavity. Shown velocity profiles correspond to the vertical plane $\phi=0$ and for cases $G>0$ when $\delta=0$.

ity, u_{x_0}, scaled with $\sin(\gamma)\cos(\gamma)(1-\delta)/(1+\delta)$ when $G>0$. Again, in this case there exists a counter flow within the porous cavity and the contour of zero velocity is at the middle of the circular section. A comparison between the basic and corrected solutions for velocity is presented in Fig. 8, where the velocity profiles on planes $\phi=0,\pi$ are shown. As the parameter λ considers the effect of the convective transport, when $\lambda=0$ the basic solution is recovered. If the thermal conductivity ratio is low the longitudinal velocity is maximum, as δ increases the longitudinal velocity diminishes and when $\delta=1$ there is no convection flow. If $\delta>1$, the longitudinal velocity changes its direction and its module augments when δ increases.

As in the previous section, the dimensionless heat flux normal to the porous cavity surface is maximum when $\delta \to 0$ and diminishes as δ increases, so that if $\delta\to\infty$ then $(\partial\theta_i/\partial r)_{r=1}\to 0$. Figure 9 shows the dimensionless heat flux normal to the cavity for different values of λ and $\delta=0.1$. It is found that the heat transfer for small Rayleigh numbers is slightly larger to that corresponding to the pure conduction condition where $\lambda=0$.

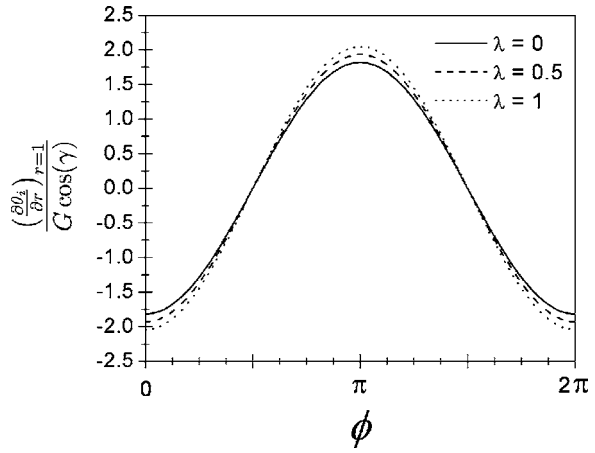

FIG. 9. Effect of the convection parameter λ on the local dimensionless heat flux normal to the porous cavity surface when $\delta=0.1$.

C. Long cavities in finite size rocks

An important feature of the asymptotic limit $\varepsilon\to 0$ already noted before is that the solution in the major part of the cavity is independent of the conditions at the ends of the cavity. This implies that the temperature and velocity distributions computed above can be applied to configurations less idealized than a long cavity in an unbounded rock. For example, the previous results are valid for a cavity at the center of a horizontal slab of rock of half-thickness $H \geqslant L\sin\gamma$. If the bases of the slab are kept at different constant temperatures T_1 and $T_2=T_1+\Delta T$, then the vertical thermal gradient is $G^*=\Delta T/2H$ far from the cavity. This fact will be used below to design a simple experiment that validates the analytical solution corresponding to a fluid-filled cavity; see next section.

IV. EXPERIMENTS FOR A FLUID-FILLED CAVITY

Conclusive velocity measurements during steady-state convection in circular cylindrical cavities are difficult in the vertical configurations ($\gamma=0$) because there exists a critical Rayleigh number [12,13,15]. In the present case, such a limitation does not occur and a simple experiment has been designed to study convection at low Rayleigh numbers in a small aspect ratio fluid-filled cavity. A cylindrical hole of radius $a=2.5\times10^{-3}$ m was drilled in a plexiglas cube of length side $2H=4.7\times10^{-2}$ m. Since the theoretical results we are going to compare with are valid even if $H=L\sin\gamma$ when $\varepsilon\ll 1$, we made the drill cross the cube from base to base at an angle $\gamma=7\pi/18$. Thus $2L=5\times10^{-2}$ m and $\varepsilon=0.1$. The inner surface of the cavity was carefully polished to allow particles visualization and it was filled with silicon oil. The plexiglas cube was kept between two blocks of cooper at different temperatures and its lateral surfaces were insulated. The thermal conductivity of the plexiglas is $k_s=0.184$ W m^{-1} K^{-1}. The properties of the silicon oil are: density $\rho=971$ kg m^{-3}, thermal conductivity $k_f=0.155$ W m^{-1} K^{-1}, thermal expansion coefficient $\beta=0.96\times10^{-3}$ K^{-1}, thermal diffusivity $\alpha=6.65\times10^{-8}$ m^2 s^{-1}, kinematic viscosity $\nu=1.25\times10^{-2}$ m^2 s^{-1}. The thermal conductivity ratio is $\delta=0.84$. The temperature distribution far from the cavity (on a surface of the plexiglas cube) was measured by using an infrared camera ThermaCAM™ PM595. The velocity field was measured with the particle image velocimetry (PIV) technique. Since the convective flow was very slow, a conventional digital video camera was sufficient for recording the particle movement. A laser beam was used as a light source. In order to improve the particle lighting, the beam was expanded into a laser sheet by means of a cylindrical prism. The laser sheet was introduced from the upper side as it is shown in the sketch of Fig. 10. The temperature of the upper copper block was 295.15 K and the temperature of the lower block was 299.15 K. The values of the Rayleigh number and the aspect ratio, which have been considered small parameters in the analysis, are $\mathrm{Ra}=0.037$ and $\varepsilon=0.1$ in these experiments. The convection parameter is $\lambda=8.1\times10^{-4}$.

After some hours were allowed to establish the desired uniform temperature gradient, one insulating wall was removed just during the short time required to measure the

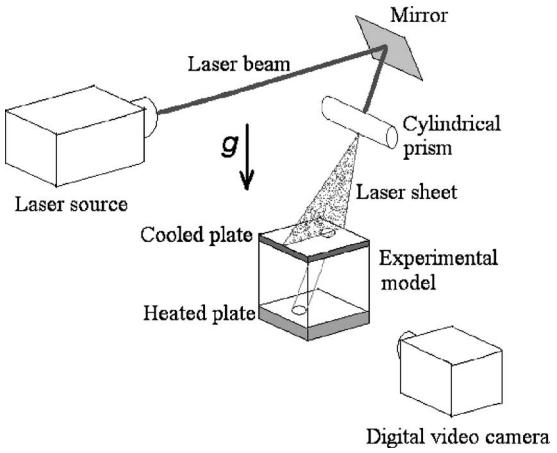

FIG. 10. Schematic of the experimental setup.

temperature distribution of the solid surface with the infrared camera. This permitted to check if the vertical temperature gradient in the solid far from the cavity was attained. Figure 11(a) shows an infrared image showing the temperature distribution on the surface of the plexiglas cube. Figure 11(b) shows three temperature profiles which corresponds to the vertical lines L1, L2, and L3 on Fig. 11(a). These images probe the existence of the constant temperature gradient in the solid far from the cavity.

Some hours after the desired temperature gradient was established, a small window of the insulation, at the central part of the cube, was removed to measure the flow through the particle motion. The digital frames obtained every 10 s

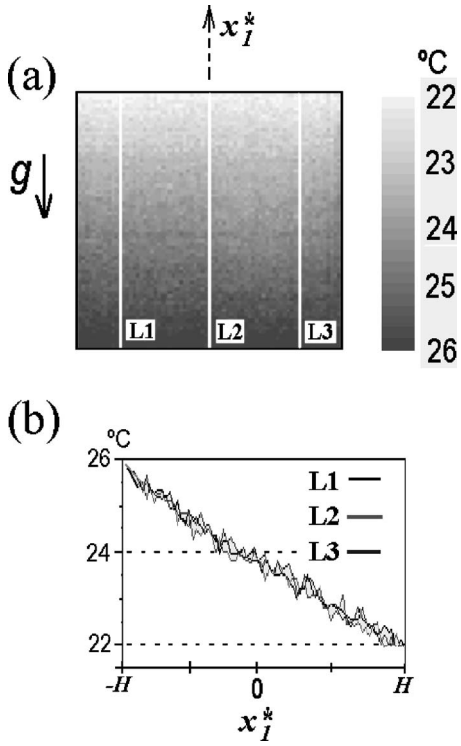

FIG. 11. (a) Infrared image showing the constant vertical temperature gradient imposed on the experimental model. (b) Vertical temperature profiles at different locations.

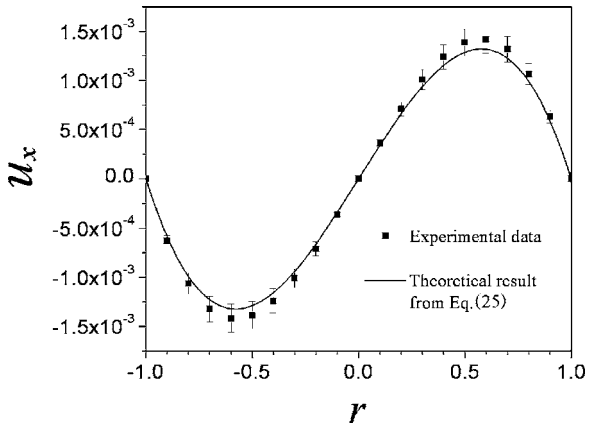

FIG. 12. Comparison between the theoretical fluid velocity profiles corresponding to planes $\phi=0$ and $\phi=\pi$ [from Eq. (25)] and the experimental data. For this case $\gamma=7\pi/18$ rad, Ra=0.037, $\varepsilon=0.1$, $\delta=0.84$, and $\lambda=8.1\times10^{-4}$. The error bars indicate an error of ±10%.

were analyzed by using a TSI™ PIV software. Figure 12 shows the good agreement found between the analytical solution and the experimental data for the time-averaged velocity of the liquid in the vertical plane $\phi=0,\pi$.

V. CONCLUSIONS

In this work we have analyzed the steady low Rayleigh number, conjugate natural convection flow in a slim, tilted cylindrical cavity which is embedded in a solid that is subject to a uniform vertical temperature gradient. We have studied the general case where the thermal conductivity of the rock is different from the thermal conductivity of the material in the cavity. The temperature distribution of the rock near the cavity is considerably affected by the sudden change in the thermal conductivity at the surface of the cavity. The coupled thermal problems within and around the cavity have been analyzed and the effect of the thermal conductivity ratio on the temperature distributions has been discussed. Convective flows which arise in the cavity due to such temperature distributions have been studied for two different cases, a fluid-filled cavity and an isotropic fluid saturated porous cavity. Closed-form analytical solutions have been obtained for the temperature in the solid and the velocity, temperature and pressure in the cavity. The solutions depend on the thermal conductivity ratio and the tilting angle of the cavity. The theoretical results show that if the Rayleigh number based on the radius of the cavity is small, then the fluid flow in cylindrical cavities is a parallel shear flow similar to the flows in long fractures or long porous layers [7,8]. It has been found that the temperature distributions are strongly dependent on the cavity aspect ratio, the tilting angle and the ratio of thermal conductivities. It is important to comment that the assumptions considered in the development of this work limit the results to ideal impervious matrices. Experiments using thermography and PIV techniques show a good agreement between the theoretical solution for the velocity and the experimental data. The present work

yields useful results for improving the estimation and comprehension of transport phenomena of interest for oil and underground water exploitation from fracture reservoir. Studies of the stability of the flow when the Rayleigh number increases are of interest to improve the understanding of this kind of flow [12]. Work on this line is in progress.

ACKNOWLEDGMENTS

F.S. acknowledges "*Programa de Estancias de Entrenamiento en Yacimientos, Instituto Mexicano del Petróleo*." A.M. acknowledges support from Spain Ministerio de Educación, Cultura y Deporte through Project No. SAB2002-0137.

[1] E. J. Shaughnessy and J. W. Van Gilder, Numer. Heat Transfer, Part A **28**, 389 (1995).
[2] M. Nagata and F. H. Busse, J. Fluid Mech. **135**, 1 (1983).
[3] O. M. Phillips, *Flow and Reactions in Permeable Rocks* (Cambridge University Press, Cambridge, England, 1991).
[4] S. H. Davies, S. Rosenblat, J. R. Wood, and T. A. Hewett, Am. J. Sci. **285**, 207 (1985).
[5] A. W. Woods and S. J. Linz, J. Fluid Mech. **241**, 59 (1992).
[6] S. J. Linz and A. W. Woods, Phys. Rev. A **46**, 4869 (1992).
[7] E. Luna, J. A. Córdova, A. Medina, and F. J. Higuera, Phys. Lett. A **300**, 449 (2002).
[8] A. Medina, E. Luna, C. Pérez-Rosales, and F. J. Higuera, J. Phys.: Condens. Matter **14**, 2467 (2002).
[9] L. W. Lake, *Enhanced Oil Recovery* (Prentice Hall, Englewood Cliffs, NJ, 1989).
[10] R. A. Lake and E. L. Lewis, J. Geophys. Res. **75**, 583 (1970).
[11] W. O. Criminale and M-P. Lelong, J. Geophys. Res. B **89**, 3581 (1984).
[12] G. Z. Gershuni and E. M. Zhukhovitskii, *Convective Stability of Incompressible Fluids* (Keter, Jerusalem, 1996).
[13] A. Jerschow, J. Magn. Reson. **145**, 125 (2000).
[14] H. H. Bau and K. E. Torrance, Trans. ASME **104**, 166 (1982).
[15] K. B. Haugen and P. A. Tyvand, Phys. Fluids **15**, 2661 (2003).
[16] L. Storesletten and M. Tveitereid, Int. J. Heat Mass Transfer **34**, 1959 (1991).
[17] S. Kimura and A. Bejan, Int. J. Heat Mass Transfer **23**, 1117 (1980).